Simulation of radar reflectivities using a mesoscale weather forecast model

Günther Haase and Susanne Crewell

Meteorological Institute, University of Bonn, Bonn, Germany

Abstract.   A three-dimensional radar simulation model (RSM) using predicted fields of a nonhydrostatic mesoscale weather forecast model, the Lokal-Modell (LM) with 2.8 km resolution, has been developed. The LM output data include the fields of the simulated hydrometeor types to study realistic cloud and precipitation fields, covering all stages of precipitation development. The RSM is able to simulate radar reflectivity measurements of any kind of radar situated within the model domain and hence allows a quick quality control of the predicted hydrometeor components. We show comparisons of simulated measurements with real measurements of a C-band radar and an X-band radar of a squall line at midlatitudes. Another application of the RSM is analytical studies using realistic physical structures of the atmosphere as given by the LM, e.g., the relation between three-dimensional reflectivity fields and the surface rain rate. The RSM is a useful tool for (1) the validation, and hence improvement, of mesoscale models and (2) the estimation of some of the errors related to the determination of the surface rain rate.

1.   Introduction

Precipitation is one of the fundamental processes within the hydrological cycle. However, as a parameter highly variable in space and time, an accurate forecast of the surface rain rate by numerical weather prediction (NWP) models is extremely difficult. A reliable forecast is desirable for several applications like evaporation studies, soil and agriculture studies, flood and erosion forecasting, and climatological statistics. Weather radar networks are nowadays operated by several national weather services and provide measurements of the radar reflectivity on regional scale and high time resolution [see, e.g., *COST 75 Action*, 1995; *Crum et al.*, 1998. Relating the measured reflectivities of the radar sampling volume to the surface rain rate can lead to substantial errors of the order of a factor of 2 [*Austin*, 1987], especially at distances larger than 100 km. In order to reduce this error, rain gauge networks are often used to adjust the rain rate retrieved from radar measurements [*Collier*, 1986]. Because of the stochastic nature of precipitation, its unknown vertical structure, and the uncertain spatial representativeness this approach can still lead to major uncertainties. Nevertheless, the method has been used for a long time because of the absence of any alternatives.

State of the art mesoscale weather forecast models have now reached a horizontal resolution ($\leq$10 km) which resolves most precipitation types, like convective and orographic rain, and which has the same spatial scale as weather radar products. For these types of models the treatment of clouds and precipitation (convection schemes) has to be evaluated and optimized. Efforts have already been made to improve mesoscale model forecasts by assimilating rainfall fields obtained from a combination of radar and rain gauge measurements [*Jones and Macpherson*, 1997]. This issue proves to be difficult because of the strong nonlinear coupling with atmospheric dynamics and is still subject of research.

Since December 1, 1999, the German Weather Service (DWD) has run its nonhydrostatic mesoscale model (Lokal-Modell (LM)) operationally. The model, which has an almost arbitrary horizontal resolution, is applicable for nowcasting, i.e., predicting severe weather situations. Radar data are well suited for the validation of high-resolution mesoscale model precipitation prediction, because only radars provide high temporal and spatial resolution over the whole model domain. To assess the model's accuracy with radar measurements, we try a new approach. Instead of converting the radar reflectivities to rain rates and comparing these with modeled precipitation fields the measurements of a radar are simulated as the beam propagates through the three-dimensional model space.

Standard radar products like plan position indicator (PPI) and range-height indicator (RHI) can be simulated from the forecast and directly compared to the radar measurement. The major motivation for the study presented here is to create an operational validation tool for quick comparisons of simulated radar reflectivities to observations of the DWD radar network. Especially in the preoperational phase of the LM, when model parameterizations were still under development, these comparisons were used to check the mesoscale precipitation patterns with radar observations on a day-to-day basis.

Radar simulation has been used in several studies to address problems of radar meteorology. *Chandrasekar and Bringi* [1987] studied the influence of varying rain drop size distributions (DSD) on the relation between radar reflectivity and the surface rain rate. In later studies [*Chandrasekar and Bringi*, 1988a, 1988b; *Chandrasekar et al.*, 1990] they extended their work to multiparameter radar, namely the error structure of differential reflectivity, X-band attenuation, and specific differential phase. *Fabry et al.* [1992] investigated the error in rainfall estimation due to changes of the measurement volume with range by means of simulation. The simulation of radar reflectivity for realistic rainfall events has been performed first by *Krajewski et al.* [1993] and in a complex extension by *Anagnostou and Krajewski* [1997]. They also simulated three-dimensional radar reflectivities using, however, a stochastic
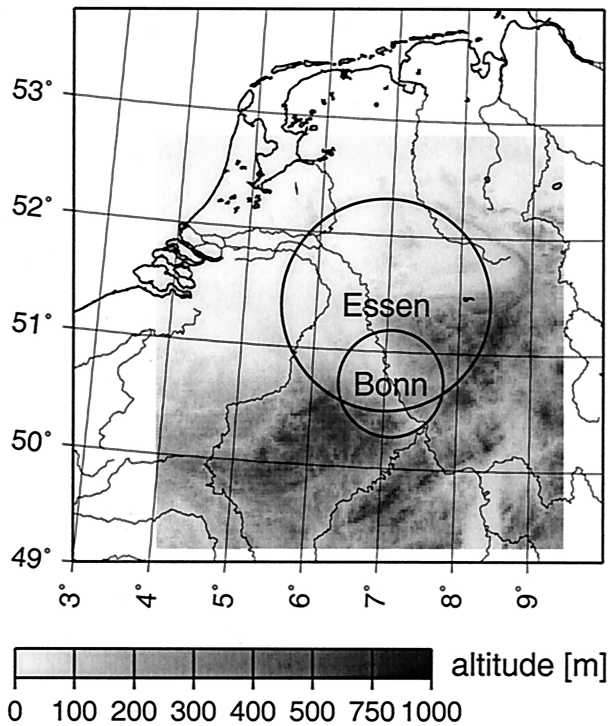
Figure 1. Location and topography of the LM domain as used in this study. The measurement radius of the C-band radar (Essen) is indicated by the 100 km circle, and that of the X-band radar (Bonn) is indicated by the 50 km circle.

space-time model of rainfall events and a statistically generated DSD. The major difference to this work is the use of mesoscale model output fields of all meteorological parameters including the different types of hydrometeors. This allows the simulation to cover a large spectrum of cloud and precipitation physics, thus attempting to be closer to reality.

The capabilities of the LM–radar simulation model (RSM) in the simulation of the radar measurement process allow one to study various sources of uncertainties in the quantitative estimation of the surface rain rate. Therefore the purpose of this paper is twofold: First, we show how the RSM can be used for the evaluation of the weather forecast model LM. Second, we use the LM-RSM chain to investigate the variability in the relation between radar reflectivity factor Z and the surface rain rate R.

The paper is organized as follows. Section 2 gives a brief summary of the LM, which output is later on used as input for the radar simulation model (RSM) described in section 3. Simulation results of a case study for February 28, 1998, are presented in section 4 and compared with the measurements of the C-band radar in Essen (DWD) and the X-band radar of the Meteorological Institute in Bonn. Section 5 comprises an analysis of the relation between the simulated radar reflectivities and the LM surface rain rate.

2. Lokal-Modell

The nonhydrostatic mesoscale Lokal-Modell [*Doms and Schättler*, 1998; *Saito et al.*, 1998], which is part of the new numerical weather prediction concept of the DWD, starts routine operation with a horizontal resolution of 7 km on December

ber 1, 1999. Two years later the resolution will be increased to 2.8 km.

For the presented work the model was run with 2.8 km horizontal resolution for a 400 km × 400 km area in the western part of Germany (Figure 1). The model domain shows moderate orographic structures on both sides of the river Rhine. The initial and boundary fields for the model are provided by the Deutschlandmodell (DM), which is a hydrostatic mesoscale model with 14 km grid size. The initialization is performed using interpolated fields of a DM analysis while boundary conditions are taken from a DM forecast run. The LM has a generalized terrain-following vertical coordinate (ζ), which divides the model atmosphere into 35 layers from the Earth's surface up to 20 hPa. The vertical resolution is highest close to the surface with <50 m vertical grid spacing and increases with altitude. The prognostic model variables are the wind vector, temperature, pressure perturbation, specific humidity, and cloud liquid water, while the geopotential height and rain and snow flux are diagnostic variables. The integration time step is 30 s, and model output, e.g., the three-dimensional fields of the variables mentioned above (on an Arakawa C-grid), is stored every forecast hour. The model physics include a level 2 turbulence parameterization, a delta-2-stream radiation transfer scheme, and a two-layer soil model. Only forecasts for which the model run was started at least 5 hours before are shown in this paper to avoid errors induced by spin-up problems of the hydrological cycle.

The model includes a grid-scale cloud and precipitation scheme as well as a parameterization of moist convection (Tiedtke mass flux scheme [*Tiedtke*, 1989]). The LM distinguishes between water contained in clouds and precipitation. To parameterize the conversion terms, cloud water is treated as a bulk phase without spectral distribution, whereas size distribution functions are specified for the precipitation phases rain and snow. These functions have only one parameter. A DSD according to *Marshall and Palmer* [1948] is assumed for rain, and a DSD according to *Gunn and Marshall* [1958] is assumed for snow. These DSDs might not be appropriate for the scale of the mesoscale model; however, within the cloud and precipitation scheme of the forecast model are many parameterizations which are on a best effort basis. The detailed structure of a typical vertical hydrometeor profile as forecasted by the LM is illustrated in Figure 2, together with the simulated radar reflectivity, also showing a bright band.

3. Radar Simulation Model

The simulation of radar reflectivities involves two steps: (1) simulation of the radar beam propagation including the effects of the Earth's curvature and atmospheric refraction and (2) determination of radar reflectivity and attenuation.

3.1. Geometry of the Radar Beam

The RSM considers the curvature of the radar beam relative to the Earth's surface. Atmospheric refraction depending on the vertical structure of temperature, humidity, and pressure is commonly parameterized by an effective Earth radius $R_{E\,\mathrm{eff}} = $ (4/3) R_E [*Doviak and Zrnić*, 1993] with R_E the true radius of the Earth. Because of the high spatial and temporal variability of humidity and temperature in the lower troposphere we calculate the local refraction index at each grid point and then use Snellius' law for calculating the radar beam curvature. The results are illustrated in Figure 3 for two different model runs,
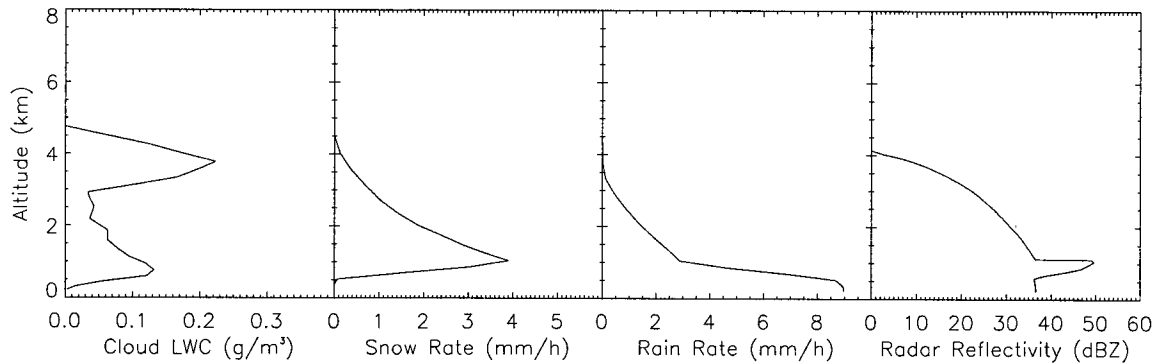
Figure 2. Vertical profiles of cloud liquid water content (LWC) and snow and rain rate as prognosticated by the LM and simulated radar reflectivity for a point 16.8 km north of Bonn on February 28, 1998 (0700 UTC).

one for a convective summer case (July 4, 1994, 1200 UTC) and one for a stratiform winter case (January 26, 1995, 1200 UTC). For two elevation angles typical for precipitation scans ($\theta = 0.5°$ and $\theta = 1.0°$), the altitude above mean sea level (asl) of the radar ray as a function of distance from the radar has been calculated for azimuth scans (PPI) with a spacing of 1.0° between the single radar rays. A high variability, especially for the lower angle and the summer case, can be observed. At a distance of 100 km from the radar the height of the beam can vary between 1.3 and 1.7 km. Differences between the parameterization and the simulation are only significant for the lower elevation angle. Here the parameterization always overestimates the height for the summer case while in the winter case

there is, at least for the more distant ranges, a systematic underestimation of height. Obviously, the use of the parameterization can lead to substantial errors in the height estimation of several hundred meters, which can be crucial, e.g., for the position of the bright band. A rough estimate of the atmospheric refraction can be obtained from a method proposed by *Fabry et al.* [1997]. They used the changes in travel time of radar waves between known ground targets (clutter) and a Doppler radar to derive the field of the near-surface refraction index.

3.2. Electromagnetic Interactions

The RSM includes the most important atmospheric interactions of an electromagnetic wave with hydrometeors, e.g.,
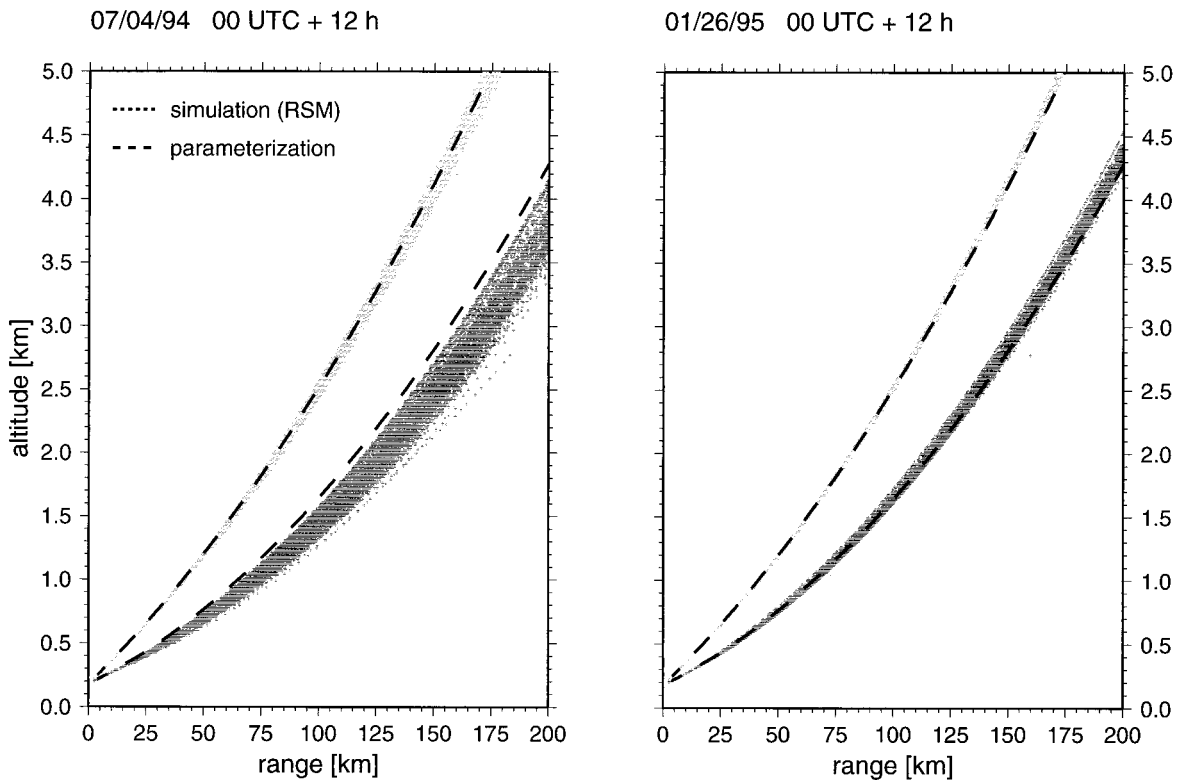
Figure 3. Altitude of the radar beam for a convective summer case (July 4, 1994) and a stratiform winter case (January 26, 1995). Two plan position indicator (PPI) scans with 1.0° resolution simulated by the RSM are shown. The scans have an elevation angle of 0.5° (dark gray) and 1.0° (light gray), respectively. The long-dashed line marks the parameterization by an effective Earth radius.

Table 1. Hydrometeor Types Considered in the RSM

Hydrometeor Type	Reference	Drop Size Distribution
Cloud water (cumulus)	*Chylek and Ramaswamy* [1982]	modified gamma
Cloud ice (cirrostratus)	*Ulaby et al.* [1981]	modified gamma
Raindrops	*Marshall and Palmer* [1948]	exponential
Snow crystals	*Gunn and Marshall* [1958]	exponential
Hail	*Douglas* [1964]	exponential

backscattering and attenuation. The three-dimensional fields of rain and snow flux as well as cloud liquid water predicted by the LM are used for calculating the volume backscattering and extinction cross sections of hydrometeors, κ_{back} and κ_{ext}, respectively, according to *Mie* [1908]. The application of the Mie formulation instead of the commonly used Rayleigh approximation gives more accurate results, especially for high frequencies and larger particles [*Ulaby et al.*, 1981]. While rain and snow are assumed to have an exponential DSD in the LM (see section 2), a cloud DSD is not resolved. Therefore the DSD for cloud liquid water has to be defined by the RSM. We take a cumulus or a cirrostratus DSD from literature depending on a temperature threshold of $-18°C$. All drop size distributions used in the RSM are listed in Table 1.

The total extinction cross section κ_{ext} is the sum of the extinction cross sections of the single hydrometeor types plus the extinction due to the absorption by the atmospheric gases, e.g., molecular oxygen, water vapor, and nitrogen. The latter

term is calculated using the millimeter-wave propagation model from *Liebe et al.* [1993]. Although several detailed parameterizations [*Ulaby et al.*, 1981; *Doviak and Zrnić*, 1993] exist, most operational measurements assume a fixed value; for example, 0.016 dB km^{-1} is currently used for the C-band DWD radar network. The error in the parameterization of the gas attenuation (Figure 4), again shown for the convective summer and the stratiform winter case, can approach 1 dB at 200 km distance compared to the fixed value for a homogeneous atmosphere. The gas absorption is systematically underestimated by the fixed value for ranges smaller than 100 km while at longer distances the effect is overestimated. The high variations, especially for the summer case, arise from the varying path lengths which the radar beam needs to pass through the warmer and more humid boundary layer due to different propagation paths (see Figure 3).

For an arbitrary radar the received power P_r (W) due to backscattering from volume-distributed incoherent scatterers is given by

$$P_r = C_{rad} \frac{1}{R^4} V_p \kappa_{back} \exp\left(-2\int_0^R \kappa_{ext}\, dR'\right), \qquad (1)$$

where C_{rad} (m^2) is the radar constant, R (m) is the range to the scattering volume, and V_p (m^3) is the pulse volume at a range R. A relationship between the received power and the radar reflectivity factor Z (mm^{6}m^{-3}), given by $Z = \Sigma_{i=1}^{N_v} d_i^6$, where d_i is the diameter of the ith particle in a unit volume v containing N_v particles, can be derived assuming only liquid particles (for snow we calculate an equivalent radius according to

07/04/94　00 UTC + 12 h

01/26/95　00 UTC + 12 h
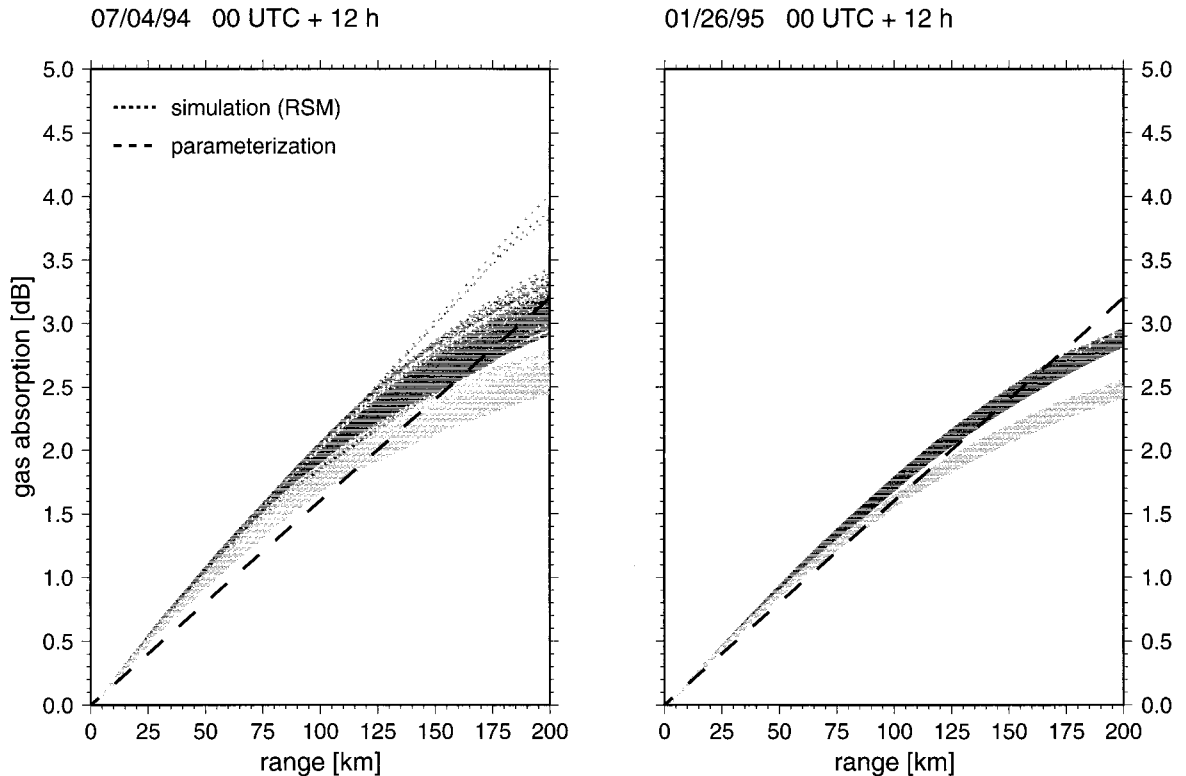
Figure 4. Gas absorption by atmospheric gases for a convective summer case (July 4, 1994) and a stratiform winter case (January 26, 1995). Two C band PPI scans with 1.0° resolution simulated by the RSM are shown. The scans have an elevation angle of 0.5° (dark gray) and 1.0° (light gray), respectively. A fixed value of 0.016 dB km^{-1} is indicated by the long-dashed line.

Ulaby et al. [1981]), pure Rayleigh scattering, and no attenuation by atmospheric gases and hydrometeors

$$P_r = C_{rad} \frac{1}{R^4} V_p 10^{-10} \frac{\pi^5}{\lambda^4} |K|^2 Z, \qquad (2)$$

where $|K|^2 = 0.93$ is the dimensionless refraction constant for water and λ is the wavelength (cm). Inserting (1) in (2) and solving for Z yields an equation for the simulated reflectivity Z_{sim}

$$Z_{sim} = 10^{10} \frac{\lambda^4}{\pi^5} \frac{1}{|K|^2} \kappa_{back} \exp\left(-2 \int_0^R \kappa_{ext} \, dR'\right). \qquad (3)$$

This is equivalent to the quantity which is shown on the common radar images and which will be simulated by the RSM along a single radar beam. Radar reflectivity is often expressed in logarithmic terms with $dBZ = 10 \log_{10}(Z)$.
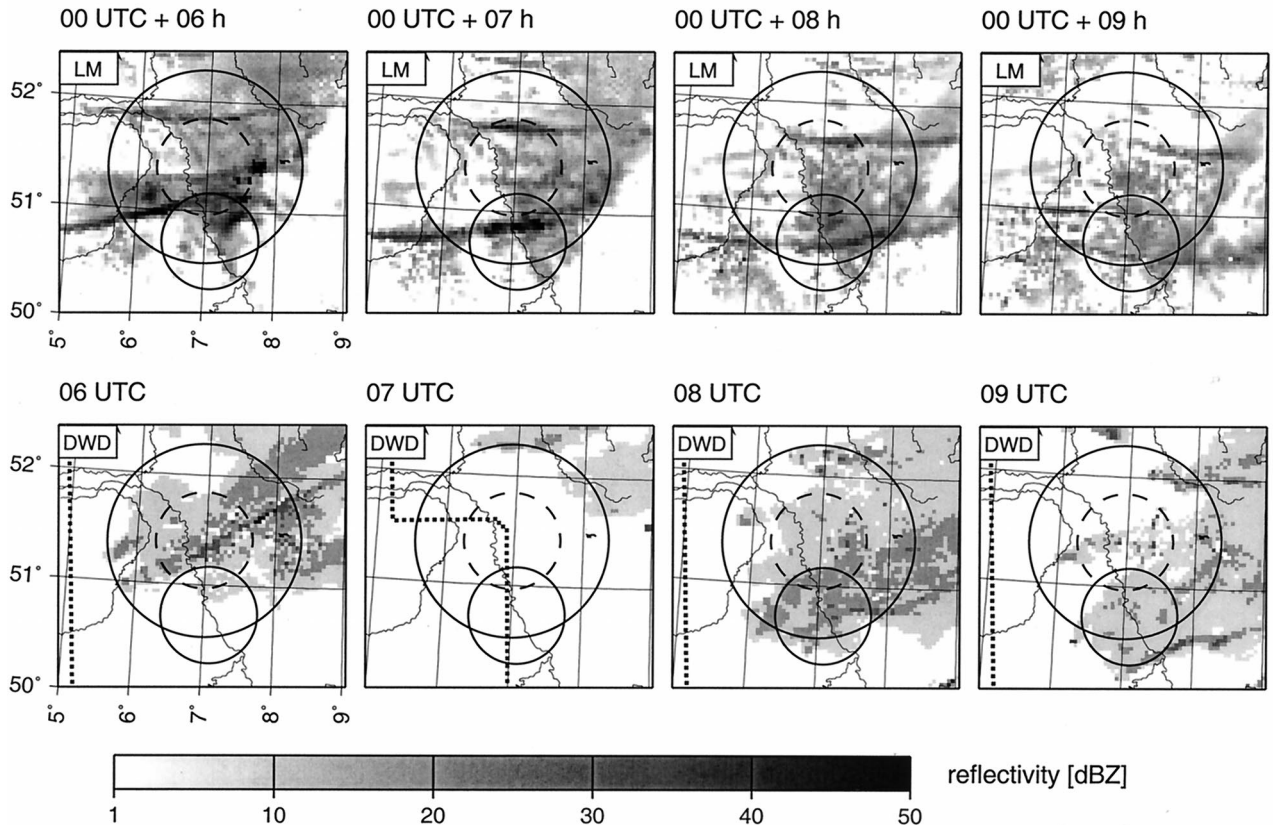
4. Case Study: February 28, 1998

As an example of weather forecast evaluation the simulated radar reflectivities from the LM-RSM chain are compared to real measurements of two different radar systems: a standard C-band radar of the DWD radar network located in Essen and an X-band radar operated by the Meteorological Institute in Bonn [*Breuer*, 1975]. For the simulation the RSM needs the frequency, the position (latitude, longitude, and altitude asl), and the scan pattern of the radar (see Table 2). While the X-band radar data were available in the original polar coordinates (azimuth, elevation, and range), the DWD's operational PN product with 4 km × 4 km horizontal resolution was taken. The PN is the national composite image mainly derived from the local precipitation scans with 0.5° elevation angle from the closest radar.

For the comparison, February 28, 1998, was chosen. On this day a cold front with associated hail crossed western Germany from NNW. The front passed Bonn at 0730 UTC, and the temperature dropped by 6 K within 40 min. The DWD radar measurement (Figure 5) at 0600 UTC shows a thin band oriented from SW to NE across the Essen radar domain. The LM, which was initialized at 0000 UTC, produces for this hour a

Table 2. Radar Parameters Used as Input for the RSM and for the Comparisons Shown in Figures 5–8

	Essen C-Band	Bonn X-Band
Frequency, GHz	5.64	9.32
Latitude, °N	6.97	7.04
Longitude, °E	51.41	50.44
Altitude asl, m	179.6	98.5
Elevation angle for PPI, deg	0.5	2.5
Horizontal resolution	4 km × 4 km	1° × 250 m
Reflectivity resolution	6 classes	0.5 dBZ

Figure 5. Comparison of radar reflectivities on February 28, 1998, at 0600, 0700, 0800, and 0900 UTC computed by the RSM from LM predictions (LM) and values measured by the C-band radar Essen (DWD) for a PPI scan with $\theta = 0.5°$. Circles indicate the radar ranges of Essen and Bonn (see Figure 2). The dotted lines mark the boundary of the DWD radar network.
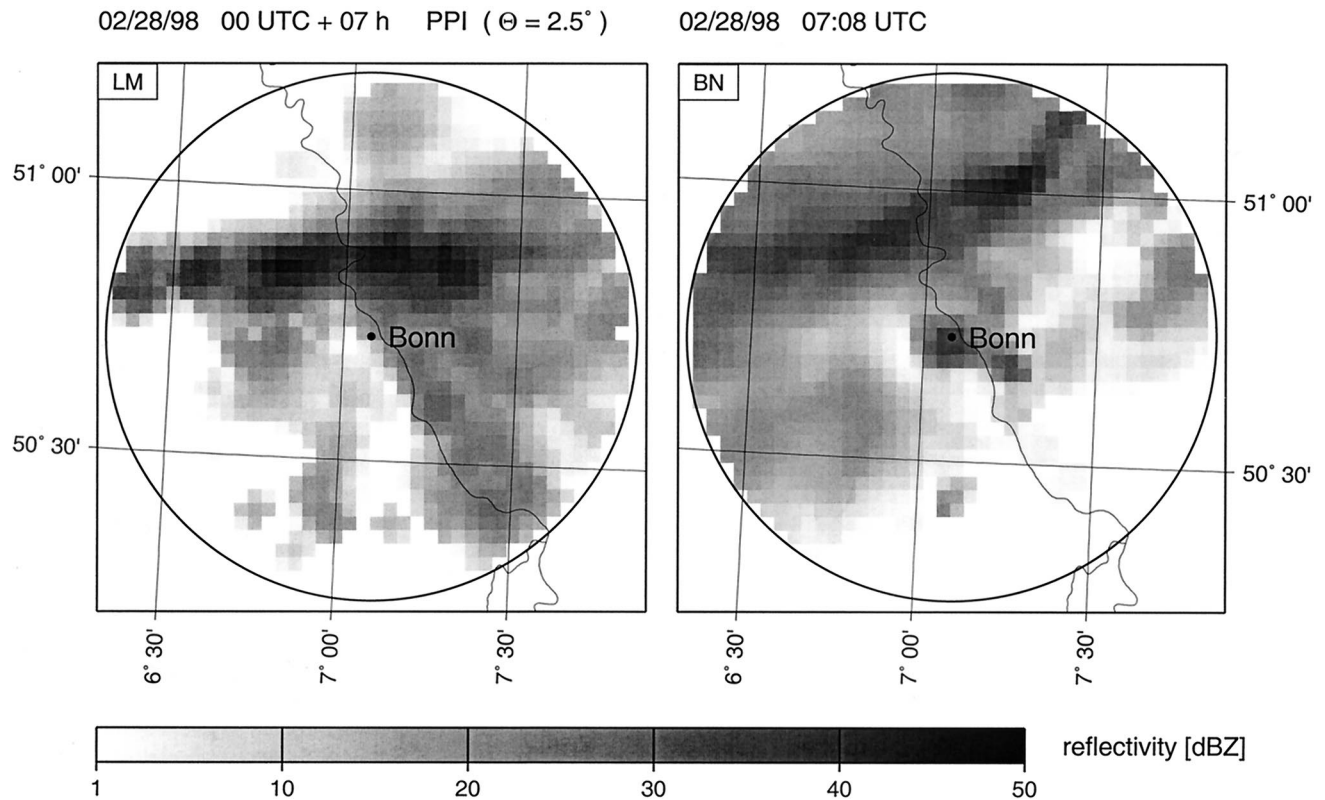
Figure 6. Comparison of radar reflectivities on February 28, 1998, at 0700 UTC computed by the RSM from LM predictions (LM) and values measured by the X-band radar Bonn (BN) for a PPI scan with $\theta = 2.5°$. The 50 km radar range is indicated.

more intense line a bit farther south oriented more zonally. Additional band structures are predicted farther north. The model successfully forecasts the dry areas in the NW and the south. During the next forecast hour the system moves southward with an intense line structure at 0700 UTC at $\sim$50.8°N. On its way south the system gets affected by topography, resulting in weaker and smaller structures. Part of the temporal variability in the intensity of precipitation structure is also caused by bright band effects. The spatial structure and temporal development of the model results agree qualitatively well with the composite image from DWD although the measured reflectivities tend to be lower. Unfortunately, the Essen radar was malfunctioning at 0700 UTC, when the line was strongest.

For 0700 UTC the LM prediction was compared to the measurements of the X-band radar in Bonn at 0708 UTC (Figure 6). For this comparison the high-resolution X-band radar data were degraded to the same 2.8 km resolution as the LM-RSM data. The LM positions the highest intensities of the line at almost the same position but can resolve the width of the frontal line with only two grid points. While the position of the front is forecasted well, the orientation differs by $\sim$30°. The model produces rain in the Rhine valley south of Bonn, not observed by the radar, which seems to be a general problem of the model. The enhanced reflectivities in the inner ring close to Bonn in the observation are artificial and due to clutter. Here it should be noted that in Figures 5 and 6 the RSM results for 0700 UTC are not identical because the reflectivities are calculated for different radar systems (see Table 2).

For the comparison of the vertical structure (Figure 7) the X-band radar data were again degraded to the LM's horizontal resolution, and both data sets were interpolated to a vertical resolution of 200 m. The RHI was simulated and measured for an azimuth angle of $\phi = 330°$, almost perpendicular to the frontal band. There is good agreement concerning the altitude of the precipitation system covering only the lower 5 km of the atmosphere. The frontal band is depicted by both, model and measurement, with a horizontal extent of $\sim$5 km (two grid points). However, the band is slightly closer to the radar site ($\sim$10 km) in the model than in the measurement. Additionally, there is no further precipitation simulated in the back of the system. The high reflectivities in the measurements close to the radar and near the ground level are clutter effects caused by the local industrial areas. Despite the rough vertical resolution a bright band with maximum reflectivities located approximately 300 m below the 0°C isotherm (solid line in Figure 7) is visible in both model and measurement.

For a more quantitative comparison between model and measurements we focus on the DWD radar data because of the better comparability of the spatial resolution. Within a radius of 100 km around Essen the simulation data set is averaged to 4 km $\times$ 4 km resolution. Because the direct comparison of radar reflectivities might be a too strong constraint, objective skill scores for the presence of precipitation are used to assess the quality of the model forecast. The occurrence of precipitation is defined by reflectivities greater than a threshold value of 1 dBZ (0.04 mm h^{-1}) as used by the DWD for winter cases. The temporal evolution of the hit rate, the false alarm rate, the tetrachoric correlation coefficient (TCC), and the area ratios for rain and no rain are shown in Figure 8. The hit rate is defined as the ratio between the number of 4 km $\times$ 4 km areas
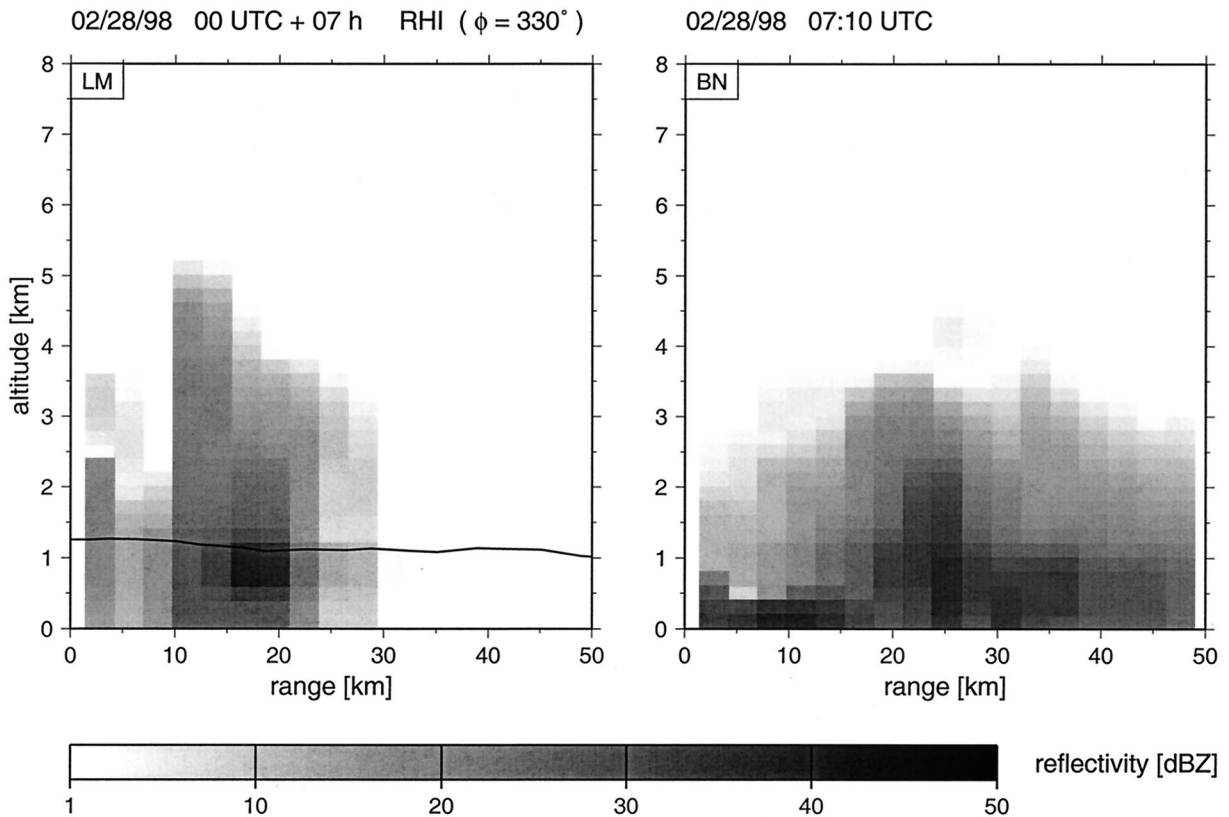
Figure 7. Comparison of radar reflectivities on February 28, 1998, at 0700 UTC computed by the RSM from LM predictions (LM) and values measured by the X-band radar Bonn (BN) for a range-height indicator (RHI) scan with $\phi = 330°$. The solid line marks the 0°C isotherm.

(pixels) with rain in both, measurement and model, divided by the total number of pixels with measured rain. The hit rate is generally high with best values higher than 75% between 0300 and ~1000 UTC. However, the hit rate does not tell anything if the false alarm rate (FAR) is not low at the same time. FAR is defined as the number of grid points with rain in the model, but not in the measurement, divided by the total number. This rate is only lower than 50% between 0300 and 0900 UTC. The low hit rate together with the high false alarm rate at the beginning of the forecast (0100 and 0200 UTC) indicate that the LM predicts the onset of precipitation too early and therefore overestimates precipitation at that time. This can be seen from the areal distribution of rain and no rain (lower part of Figure 8), where the area of rain simulated by the LM is much too high by over 400%. In general, the LM overestimates the area where precipitation ocurrs. Only at 0800 UTC is the partitioning between rain and no rain areas forecasted well with both values close to 100%. The TCC coefficient is a score which combines the information of hit and false alarm rate. If TCC = 1, radar and model are identical at each pixel, while TCC = 1 means no agreement at all. Only in the earlier forecast stage is TCC negative, which can possibly be attributed to spin-up effects of the hydrological cycle. The positive values during the further forecast indicate good results.

5. Analysis of the *Z-R* Relation

The LM-RSM chain can also be used as a tool to investigate radar meteorological problems. The most important aspect is the relation between the radar reflectivity factor Z measured by the radar for a pulse volume within the three-dimensional space and the rain rate R at the ground. Because of the complexity of the precipitation process this relation is nonunique (see, for example, the more than 70 relations listed by *Battan* [1973]). The LM-RSM combination is well suited to study these effects because of the mesoscale model's capability to simulate a realistic temporal development of the three-dimensional fields of hydrometeors. For a PPI scan at $\theta = 0.5°$ on February 28, 1998, 0700 UTC (see Figure 5), a scatterplot of simulated radar reflectivities against surface rain rates >0.1 mm h^{-1} is shown in Figure 9. Reflectivity values cover the typical range from −20 to 50 dBZ while the surface rain rate does not exceed 15 mm h^{-1} in this case. The solid line marks the least squares regression of the form $Z = aR^b$ for all simulation points within a 100 km radius of the Essen radar. The regression was performed using the logarithmic values of Z and R. Additionally, the relation to the coefficients ($a = 206$, $b = 1.56$), as implicitly used in the LM by its fixed terminal velocity and form of the drop size distribution (see section 2), is shown. These coefficients are close to the ones ($a = 200$, $b = 1.6$) proposed by *Marshall et al.* [1955], which is the most commonly used *Z-R* relation for midlatitude cold frontal events. There is a pronounced deviation from a simple *Z-R* relation due to attenuation effects and changes in the hydrometeor distribution between the elevated scattering volume and the surface. While attenuation reduces the radar reflectivity and therefore leads to a vertical downward shift of the points in Figure 9, a variable rain rate profile results in a horizontal shift.
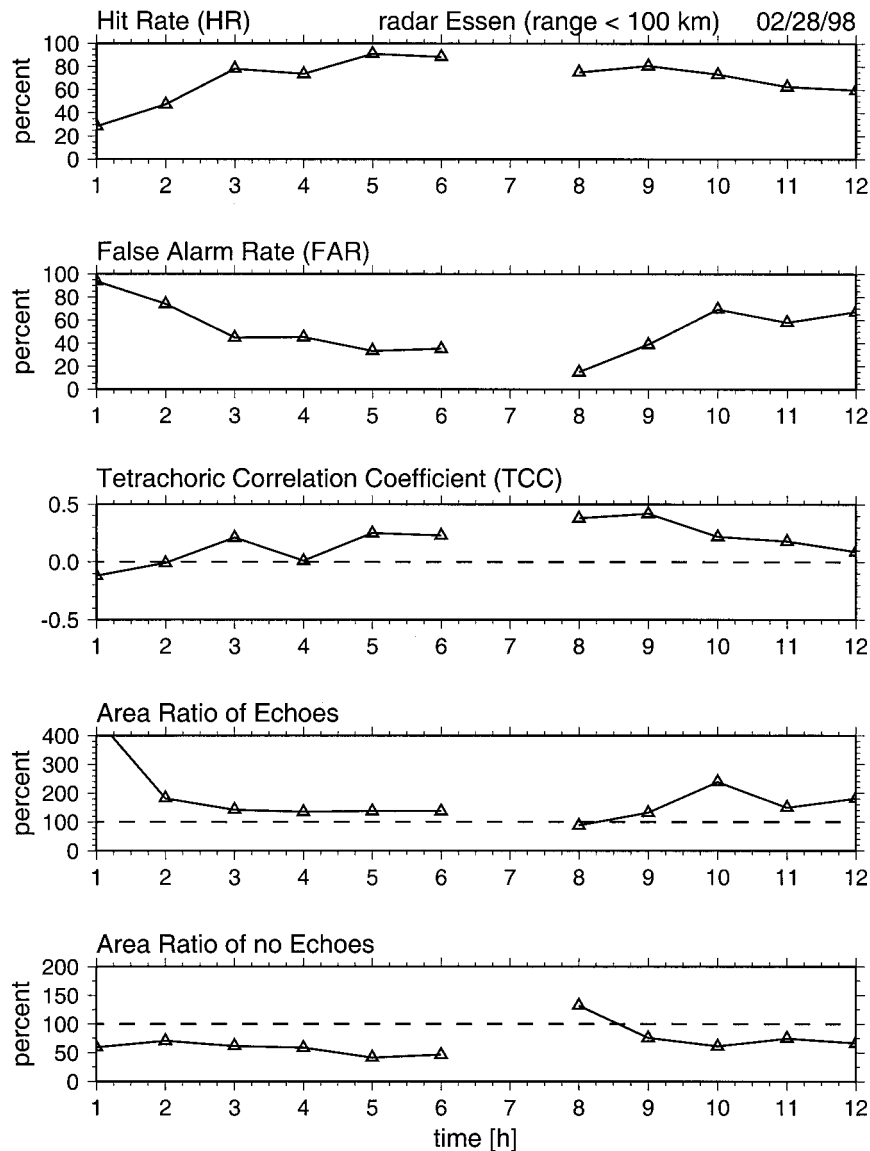
Figure 8. Objective skill scores for the prediction quality of the LM during the 12 forecast hours on February 28, 1998, derived by comparison to DWD radar measurements.

The amount of scatter in Figure 9 is comparable to the model results shown in the study by *Anagnostou and Krajewski* [1997] (hereinafter referred to as AK97; their Figure 8). However, real observations (see Figure 7 of AK97) show a significantly higher amount of scatter, suggesting that both models miss important sources of variability: (1) The variability in the DSD is taken into account by AK97 using a statistically parameterized three-parameter gamma-type DSD [*Krajewski et al.*, 1993], while our model (LM-RSM) assumes an exponential relation with the rain rate as the only free parameter, which will lead to a smaller variability in our results. (2) The detailed vertical structure of the hydrometeor profiles and their realistic spatial and temporal evolution as simulated by the LM-RSM combination will not be evident in AK97. (3) The subgrid natural rainfall variability is depicted in the AK97 simulations, since their stochastic model could generate rainfall fields with high spatial resolution (100–300 m). The LM resolution of 2.8 km is too coarse for that. However, a high-resolution LM version (~100 m) is under development and will be used in the

future to investigate this effect. For this purpose it is necessary to include the antenna pattern into the RSM.

We further investigated the influence of the different hydrometeor classes, especially the occurrence of mixed phases in one radar measurement (Figure 10). With low-level clouds, the 0°C isotherm at ~1 km height, and snow reaching down to ~500 m asl the majority of backscattering volumes are mixtures of cloud water, rain, and snow (Figure 10a). There is a high amount of scatter even if only points closer than 50 km to the radar are regarded. This suggests a change in the hydrometeor profiles even in the lowest atmospheric levels (approximately below 450 m), possibly caused by evaporation, diffusional growth, or conversion to a different hydrometeor type. Points with distances farther than 50 km from the radar have an even higher variability with enhanced reflectivities due to bright band effects and lower reflectivities resulting from a pronounced decrease in rain rate with height (see Figure 2). When only a combination of rain and snow is regarded (Figure 10b), about the same scatter as in Figure 10a can be observed
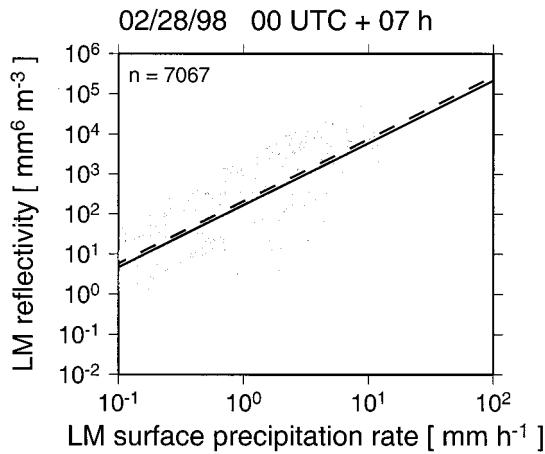
Figure 9. Simulated radar reflectivity Z versus LM surface precipitation rate R for the C-band radar located in Essen (PPI scan with 0.5° elevation angle on February 28, 1998, 0700 UTC, as in Figure 5). Only points within a 100 km range are considered. The solid line marks the least squares regression of the form $Z = aR^b$. The dashed line is based on the coefficients ($a = 206$, $b = 1.56$) implicitly used in the LM.

because of the low radar reflectivity and attenuation of cloud liquid water. In general, the reflectivities are higher when snow is present compared to cases with rain only (Figure 10c) and rain and cloud water (Figure 10d) because of the enhancement resulting from a bright band.

If only rain is considered, a surprising two-line structure with an offset of ~4 dBZ is evident (Figure 10c). This is caused by the occurrence of two rain areas: one close to the radar (~15 km), which appears as a nearly straight line, and a second one more distant from the radar (~90 km). Attenuation at the C-band frequency due to rain does not exceed 1 dBZ in this case (low rain rates) and hence cannot explain the downward shift of the Z-R relation for the second rain area. Indeed, this is a horizontal shift due to the change of rain rate with height, which affects the second area more strongly where the radar observations are at higher altitudes. Additionally, the second area is in the back of the strong frontal zone and belongs to another air mass which is characterized by higher clouds, no snow, and a different rain profile. It should be noted that the straight line structure results from the assumption of a fixed DSD for rain.

The interpretation of Figure 10 has revealed a high variability due to spatial variations. We also investigated the temporal variations during the passage of the frontal band over the area 50 km around Bonn (Figure 11) for the 12 hour forecast run. During this time the system completely passes the area, showing the maximum in the mean area precipitation between 0600 and 0800 UTC. To calculate the surface precipitation field which would be derived from radar measurement, we applied the fixed Z-R relation for rain to the simulated azimuth scan (see Figure 6 for 0700 UTC). Then we compared the surface precipitation forecasted by the LM and the hypothetical radar precipitation calculated this way for each time step (one hour).
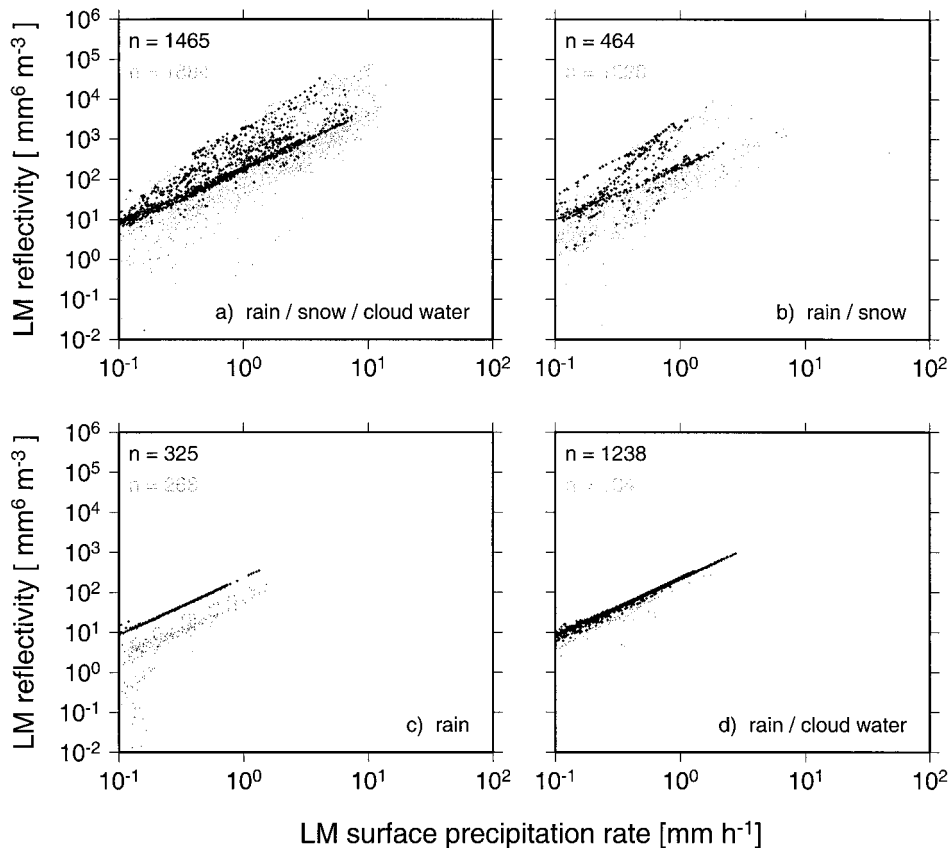
Figure 10. Same as Figure 9, except that simulation results are shown for scattering volumes consisting of (a) rain, snow, and cloud water, (b) rain and snow, (c) rain, and (d) rain and cloud water. Two range intervals are shown: 0–50 km (dark gray) and 50–100 km (light gray).
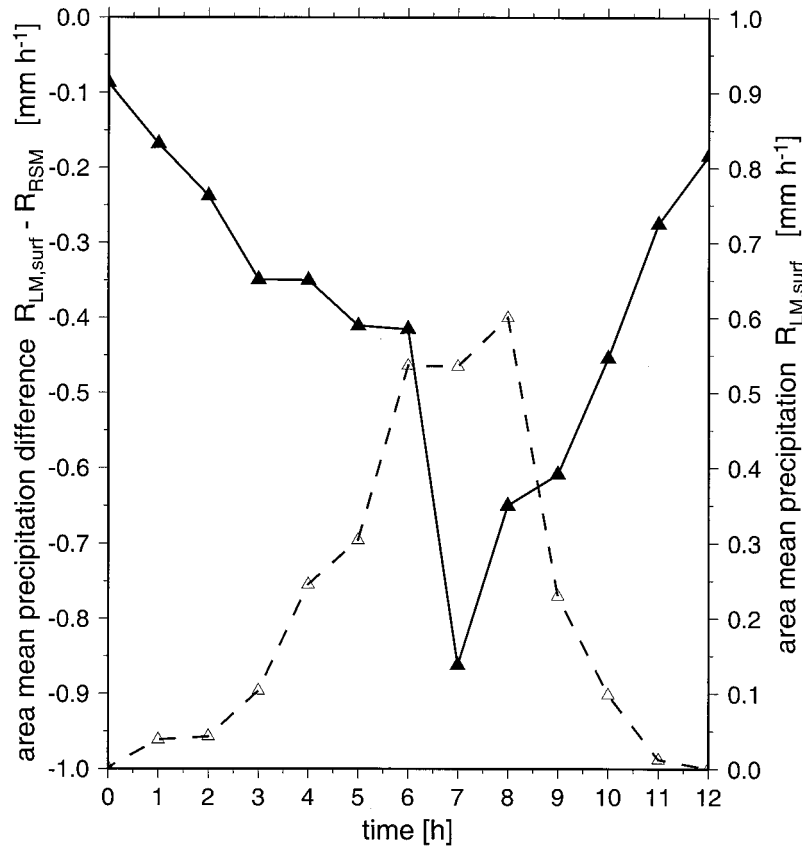
Figure 11. Temporal development of the area mean difference between $R_{LM,surf}$ and R_{RSM} on February 28, 1998. $R_{LM,surf}$ is the surface precipitation rate as forecasted by the LM, and R_{RSM} is derived by converting the reflectivities simulated for the X-band radar Bonn (Figure 6) to rain rates according to *Marshall and Palmer* [1948]. The area mean precipitation is shown by the dashed line.

During the whole run the precipitation is overestimated by the hypothetical radar. This is even the case for the first time step, when the LM has no surface precipitation yet. The reason for that is the occurrence of strongly scattering hydrometeors at higher levels of the atmosphere, which are seen by the radar. Here it should be noted that the first time steps are still in the spin-up phase of the mesoscale model. The strongest disagreement is evident at 0700 UTC due to the presence of a strong bright band (see Figure 7).

6. Conclusion

A radar simulation model (RSM) has been developed to calculate radar reflectivities from the output of a mesocale weather forecast model, the Lokal-Modell (LM), with a horizontal resolution of 2.8 km. Reflectivities, which would be observed by two radar systems differing in frequency, position, and scan pattern, were calculated. Basically, the model is capable of simulating any kind of radar. The horizontal resolution is sufficient for comparison with the radar products derived from standard radar networks. However, for a quantitative comparison with high-resolution radar data, LM model runs with a higher resolution are desirable.

The comparison of radar reflectivities predicted by the LM-RSM combination with measured reflectivities is acceptable for the case investigated in this study. The direct comparison of radar reflectivities, measured and forecasted, reduces some of the uncertainties pertinent to the comparison of modeled with

radar-derived precipitation. When the radar measurement is converted into a rain rate, conventionally, by a simple Z-R relation, the propagation of the radar beam in the three-dimensional space as well as the effects of attenuation by hydrometeors and atmospheric gases are neglected. Comparing forecast and measurement by means of objective skill scores offers the opportunity to easily assess the quality of the weather forecast model. The comparison (see Figure 8) shows the example of a good forecast of the distribution of rain and no rain within the model domain, which is of high importance for nowcasting applications. This was not the case for earlier model versions of the LM, when, for example, no convection scheme was implemented. Since December 1, 1999, the LM with a resolution of 7 km is operationally run by the German Weather Service (DWD), and the RSM will be used in parallel for the ongoing validation. The LM with a 2.8 km resolution (as used in this study) is scheduled to go into operational mode approximately in 2001. The ongoing development of this model version will involve the RSM.

The LM-RSM's quality to simulate realistic weather developments, e.g., the temporal development of the three-dimensional fields of hydrometeor types, can be used to study various aspects of radar meteorology, the most fundamental one being the relation between the radar reflectivity and the surface rain rate. The scatter in the Z-R relation for the case presented here, a typical cold front passage at midlatitudes, is high and mostly caused by changes in the profiles of rain and

snow. However, the scatter is not as high as shown in real observations and is probably due to the fixed form of the drop size distributions (DSD) and the missing subgrid variability in the LM. The assumption of fixed DSDs is part of the LM's cloud and precipitation scheme as developed by the DWD. In principle the output of any spectrally resolved model could be used for the RSM.

In comparison to a radar simulation study [*Anagnostou and Krajewski*, 1997], which includes variations of the DSD and subgrid variability, we still get about the same scatter. This is due to detailed vertical variability provided by the mesoscale model and emphasizes the importance of including this effect in radar simulation studies, especially when midlatitude frontal systems are concerned. The issue of subgrid variability is not so important for the case of a frontal band, presented in this study. This can be seen from high-resolution X-band radar measurements, but it could be quite significant for convective situations.

Another limitation of the RSM is the approximation of the radar beam as a pencil beam. We are currently integrating the antenna pattern into the model, which will also help to address clutter-related problems.

The LM in its current version does not resolve the particle spectrum and has only a crude parameterization of the ice phase. Further model improvements can easily be incorporated into the RSM.

References

Anagnostou, E. N., and W. F. Krajewski, Simulation of radar reflectivity fields: Algorithm formulation and evaluation, *Water Resour. Res.*, *33*, 1419–1428, 1997.

Austin, P. M., Relation between measured radar reflectivity and surface rainfall, *Mon. Weather Rev.*, *115*, 1053–1070, 1987.

Battan, L. J., *Radar Observations of the Atmosphere*, Univ. of Chicago Press, Chicago, Ill., 1973.

Breuer, L. J., Results of four years measurements of radar reflectivity and rainfall rate at Bonn, Germany, paper presented at 16th International Conference on Radar Meteorology, Am. Meteorol. Soc., Houston, Tex., 1975.

Chandrasekar, V., and V. N. Bringi, Simulation of radar reflectivity and surface measurements of rainfall, *J. Atmos. Oceanic Technol.*, *4*, 464–478, 1987.

Chandrasekar, V., and V. N. Bringi, Error structure of multiparameter radar and surface measurements of rainfall, part I, Differential reflectivity, *J. Atmos. Oceanic Technol.*, *5*, 783–795, 1988a.

Chandrasekar, V., and V. N. Bringi, Error structure of multiparameter radar and surface measurements of rainfall, part II, X-band attenuation, *J. Atmos. Oceanic Technol.*, *5*, 796–802, 1988b.

Chandrasekar, V., V. N. Bringi, N. Balakrischnan, and D. S. Zrnić, Error structure of multiparameter radar and surface measurements of rainfall, part III, Specific differential phase, *J. Atmos. Oceanic Technol.*, *7*, 621–629, 1990.

Chylek, P., and V. Ramaswamy, Simple approximation for infrared emissivity of water clouds, *J. Atmos. Sci.*, *39*, 171–177, 1982.

Collier, C. G., Accuracy of radar estimates by radar, part I, Calibration by telemetring raingauges, *J. Hydrol.*, *83*, 207–223, 1986.

COST 75 Action, *COST 75 Weather Radar Systems*, edited by C. G. Collier, *Rep. EUR 16013 EN*, 814 pp., Eur. Comm., Brussels, 1995.

Crum, T. D., R. E. Saffle, and J. W. Wilson, An update on the NEXRAD program and future WSR-88D support to operations, *Weather Forecasting*, *13*, 253–262, 1998.

Doms, G., and U. Schättler, The nonhydrostatic limited-area model LM (Lokal-Modell) of DWD, part I, Scientific documentation, 160 pp., Ger. Weather Serv. (DWD), Offenbach, Germany, April 1998.

Douglas, R. H., Hail size distributions, paper presented at 1964 World Conference on Radio Meteorology, Am. Meteorol. Soc., Boulder, Colo., 1964.

Doviak, R. J., and D. S. Zrnić, *Doppler Radar and Weather Observations*, 2nd ed., 562 pp., Academic, San Diego, Calif., 1993.

Fabry, F., G. L. Austin, and D. Tees, The accuracy of rainfall estimates by radar as a function of range, *Q. J. R. Meteorol. Soc.*, *118*, 435–453, 1992.

Fabry, F., C. Frush, I. Zawadzki, and A. Kilambi, On the extraction of near-surface index of refraction using radar phase measurements from ground targets, *J. Atmos. Oceanic Technol.*, *14*, 978–987, 1997.

Gunn, K. L. S., and J. S. Marshall, The distribution with size of aggregate snowflakes, *J. Meteorol.*, *15*, 452–466, 1958.

Jones, C. D., and B. Macpherson, A latent heat nudging scheme for the assimilation of precipitation data into an operational mesoscale model, *Meteorol. Appl.*, *4*, 269–277, 1997.

Krajewski, W. F., R. Raghavan, and V. Chandrasekhar, Physically based simulation of radar rainfall data using a space-time rainfall model, *J. Appl. Meteorol.*, *32*, 268–283, 1993.

Liebe, H. J., G. A. Hufford, and M. G. Cotton, Propagation modeling of moist air and suspended water/ice particles at frequencies below 1000 GHz, paper presented at AGARD 52nd Special Meeting of the Panel on Electromagnetic Wave Propagation, Adv. Group Aerosp. Res. Dev., Palma de Mallorca, Spain, 1993.

Marshall, J. S., and W. M. Palmer, The distribution of raindrops with size, *J. Meteorol.*, *5*, 165–166, 1948.

Marshall, J. S., W. Hitschfeld, and K. L. S. Gunn, Advances in radar weather, *Adv. Geophys.*, *2*, 1–56, 1955.

Mie, G., Beiträge zur Optik trüber Medien, speziell kolloidaler Metallösungen, *Ann. Phys.*, *25*, 377–445, 1908.

Saito, K., G. Doms, U. Schättler, and J. Steppeler, 3-D mountain waves by the Lokal-Modell of DWD and the MRI mesoscale nonhydrostatic model, *Pap. Meteorol. Geophys.*, *49*, 7–19, 1998.

Tiedtke, M., A comprehensive mass flux scheme for cumulus parameterization in large-scale models, *Mon. Weather Rev.*, *117*, 1779–1799, 1989.

Ulaby, F. T., R. K. Moore, and A. K. Fung, Microwave Remote Sensing, Active and Passive, vol. 1, 456 pp., Addison-Wesley-Longman, Reading, Mass., 1981.

S. Crewell and G. Haase, Meteorological Institute, University of Bonn, Auf dem Hügel 20, 53121 Bonn, Germany. (screwell@uni-bonn.de; ghaase@uni-bonn.de)